Regular Article

Evaluation on Cytotoxicity of Natural Rubber Latex Nanoparticles and Application in Bone Tissue Engineering

Mitsuru Furuya, Naoki Shimono, Kazuyuki Yamazaki, Ryota Domura, and Masami Okamoto*

Advanced Polymeric Nanostructured Materials Engineering, Graduate School of Engineering, Toyota Technological Institute, 2–12–1 Hisakata, Tempaku, Nagoya 468–8511, Japan
*Corresponding Author: okamoto@toyota-ti.ac.jp

Received May 25, 2017; Accepted July 28, 2017

Abstract To broaden the knowledge of cytotoxicity of natural rubber latex (NRL) nanoparticles we for the first time examined the latex biocompatibility in vitro against mouse calvaria preosteoblastic cells (MC3T3-E1) and human alveolar basal epithelial (A549) cells. For NRL nanoparticles, the half maximal inhibitory concentration (IC_{50}) value for MC3T3-E1 cells is one order of magnitude higher in toxicity as compared to that of A549 cells (3.99 mg/mL for MC3T3-E1 and 0.33 mg/mL for A549 cells). Owing to fractionation of NRL nanoparticles by ultra-centrifuge, the effect of the non-rubber constituents on the cytotoxicity was clarified. The suppression on the proliferation for A549 cells incubated with NRL nanoparticles was demonstrated by the cell cycle distribution. The in vitro study on osteogenic differentiation and expressions of proteins and characteristic genes of MC3T3-E1 cells demonstrated the promising results of the NRL nanoparticles for application in bone tissue engineering.

Keywords Natural rubber latex, MC3T3-E1 cells, A549 cells, cytotoxicity, osteogenic differentiation

Introduction

Natural rubber latex (NRL) is a type of high molecular weight polymeric substance. Currently, more than 90% of NRL comes from one single tropical tree species—*Hevea brasiliensis* (para rubber tree). Recently, promising results in the use of NRL from *Hevea brasiliensis* rubber tree to produce replacement and regeneration tissues has been reported[1–3]. Among them, wound healing in cutaneous tissues, eardrum replacement, bone regeneration, and dental alveolus replacement afford a unique means to repair or replace the failing organs or tissues[2]. Nevertheless, little attention has been paid to pharmacological potential activity of NRL as nanoparticle. The reason behind this is well explored as allergic problems in some sensitive individuals, which cause immediate hypersensitivity, mediated by immunoglobulin E (IgE) antibodies to specific proteins (Hevb1 and Hevb3) in the latex. On the one hand, however, the prevalence of latex allergy in population is believed to be very low[4, 5].

The primary particle of NRL is around 100–300 nm in diameter[6], which is promising nanoparticles used in biotechnology including pharmaceutics and medicines. We are interested in the investigation of an anticancer activity of NRL with bioactive properties of natural products. In this regard, only a few studies have evaluated the safety and potential adverse effect on living system[6–8]. In addition, the possible reason behind the mechanism of interacting with living cells is not well explored in the literature. Furthermore, most studies have observed cytotoxicity only at high concentrations (100 mg/mL)[6]. Further information on the potential cytotoxicity of the NRL particles and their mechanisms of toxicity are needed to fully understand their hazards.

In this work, we examined the latex cytocompatibility in vitro against cultured human lung carcinoma (A549) cells to emphasize the anticancer effects of NRL particles. We also compared the cytotoxic effect of NRL on mouse calvaria preosteoblastic cells (MC3T3-E1). In order for NRL nanoparticles to be employed in bone regeneration, we have used MC3T3-E1 cells to examine in vitro osteoconductivity. These cells behave similar to osteoblast progenitors in that they differentiate in osteoblasts that synthesize bone matrix collagen[9]. With this in mind, an in-depth understanding of cell differentiation may bring a new perspective to regenerative medicine including new bone re-

generation and cartilage therapy. To the best of our knowledge, there are no reports on the osteogenic differentiation of preosteoblastic cells incubated with NRL nanoparticles.

Using MC3T3-E1 osteoblastic-like cells, in this study, we examined the osteogenic differentiation and expressions of proteins and characteristic genes of mature osteoblast.

Materials and methods

NRL and characterization

The solution sample (solid content of 35.4 wt%) was provided by Sumitomo Riko Co. Ltd., Japan and was not further purified for use. It was stabilized (pH 11.3) using an ammonia solution (0.5 wt% in 100 mL of latex, which corresponds to less than 1 wt% of solid NRL). The surface charge characteristics of NRL nanoparticles in water (0.01 wt%) were determined by electrophoresis (Zetasizer Nano ZS, Malvern Instruments, UK) by the technique of laser Doppler anemometry adjusting the pH of the suspension in the range of 2–12 using dilute HCl and NaOH (Nacalai-Tesque). The average diameter of the nanoparticles was measured by dynamic light scattering (DLS) using Zetasizer Nano ZS (wavelength=532 nm). The dynamic information can be retrieved by examining the autocorrelation function $g(t)$ of the time-dependent intensity[10].

The morphology was observed through field emission scanning electron microscope (FE-SEM: SU6600, Hitachi Ltd.). The operated accelerating voltage was 15 kV and the specimens were coated with a thin layer of gold and palladium (Au/Pd 6:4) with a thickness of ~20 nm on copper grids with 200 mesh size, and then water removed by placing filter paper at the edge of the grids.

NRL nanoparticle is composed of three layers structure composed of *cis*-1, 4-polyisoprene as a core, lipids and proteins as surfaces thin layers. To fractionate the NRL suspension (0.1 wt%) into three components polymeric substance (*cis*-1, 4-polyisoprene) was collected after ultra-centrifuge at 10^5 g for 30 min and the supernatant (protein, polypeptides and organic acids) was collected after centrifuge at 5×10^5 g for 120 min using an ultra-centrifuge system (Optima MAX-XP, Beckman Coulter K.K. Japan). Subsequently, freeze-drying (FDU-2200, Eyela Ltd.) was performed under 20 Pa at −80 °C.

Fourier transform infrared (FTIR) spectroscopic imaging measurements were preformed using a Perkin-Elmer Spectrum Spotlight 400 Microscope System. This system is equipped with a liquid N_2 cooled Mercury-Cadmium-Telluride MCT detector. To construct FTIR maps, spectra were collected in continuous scan mode for sample area of $200\times200\,\mu m^2$ with a resolution of 1.65 μm/pixel by one scan for each spectrum of the specimens under the Ge attenuated total reflectance (ATR) crystal. Spectra were collected from 4000–680 cm^{-1} with a resolution of 8 cm^{-1} and integrated by taking the areas under the curve between the limits of the peaks of interest. Data acquisition was carried out by means of the Spotlight software package.

X-ray fluorescence analysis was done using an energy dispersive spectroscopy (EDX) (EDX-7000, SHIMADZU, Japan) equipped with Rh Kα radiation operated at 0.3 mA and 40 kV.

In vitro cell culture and cell viability

MC3T3-E1 mouse calvaria preosteoblastic cells obtained from ATCC were cultured in Alpha Minimum Essential Medium (α-MEM) (Gibco®, Life Technologies) at pH 7.40 supplemented with 10% (v/v) fetal bovine serum (FBS) (Gibco®, Life Technologies) and 1% antibiotic-antimycotic mixture (Nacalai-Tesque). Upon reaching confluence, cells were cultured on 10 cm dishes in an atmosphere of 5% CO_2 and 95% relative humidity at 37°C. MC3T3-E1 cells at 2–4 passages were used in the experiment.

Human lung carcinoma A549 (ATCC) cells were used as a cancer cell and cultured in RPMI-1640 (Wako Pure Chemical Industries) supplemented with 10% FBS including 1% antibiotic-antimycotic mixture. Upon reaching confluence, cells were cultured on 10 cm dishes in an atmosphere of 5% CO_2 and 95% relative humidity at 37°C. A549 cells at 2–5 passages were used in the experiment.

The cells were seeded in 96-well plates at a cell concentration of 2.0×10^4 cells/cm^2 in 100 μL of media and cultured for 24 h. NRL suspensions at different concentrations (ranged from 10 μg/mL to 100 mg/mL) were diluted with each complete culture medium and added to each well. After incubation for 24 h in an atmosphere of 5% CO_2 and 95% relative humidity at 37°C, the cell viability was assessed by WST-8 assay (Dojindo) according to manufacturer's instructions. The WST-8 colorimetric test is measuring the activity of intracellular dehydrogenase activity, which is proportional to living cells. The optical density was read on a Multiskan FC (Thermo Fisher Scientific) at 450 nm for the absorbance and at 650 nm for the subtract background absorbance, respectively. The half maximal inhibitory concentration (IC_{50}) values at 24 h were estimated from the dose-response curves.

Flow cytometry

A549 cells were seeded in 24-well plates at a density of 2.0×10^4 cells/cm^2 and incubated for 24 h, then the cells

were exposed to 330 μg/mL (equal to IC_{50} for A549) for 6 and 24 h. After incubation, the cells were washed twice with cold PBS and collected by trypsinization. Then the cells were washed and centrifuged twice with PBS again, and fixed 10 mL 70% EtOH at 4°C for 2 h. Then the cell were centrifuged and washed twice with 5 mL phosphate-buffer saline (PBS, Nacalai Tesque), resuspended in propidium iodide (PI, Sigma-Aldrich) solution, i.e., 0.25 mg/mL RNAse in PBS, pH 7.4 for 37°C for 30 min plus 50 mg/mL PI for 30 min in darkness at room temperature. The cell cycle distribution was analyzed by a flow cytometer (BD Accuri™ C6, Becton Dickinson Biosciences Ltd.).

Differentiation

For osteogenesis, MC3T3-E1were seeded at a density of 4.0×10^4 cells/cm^2 in 200 μL of osteogenic medium and cultured with NRL nanoparticles (1.0 mg/mL). The effect of NRL on cell differentiation was determined for 21 days in osteogenic medium, consisting of α-MEM, 10% FBS, 1% (v/v) ascorbic acid (TaKaRa), 0.2% (v/v) Hydrocortisone (TaKaRa), 2% (v/v) β-Glycerophosphate (TaKaRa) and 1% antibiotic-antimycotic mixture. The medium was changed with a fresh one every 3 days, 7 times during the 20 days induction.

For the calcium deposition, after 20 days, the osteoinduction of the MC3T3-E1 cells in osteogenic culture was analyzed by measuring the absorption of treated cells by Alizarin Red staining (PG Research) according to the manufacture's instructions. The optical density at 450 and 650 nm, for the subtract background absorbance, were read using a microplate spectrophotometer (Multiskan FC, Thermo Fisher Scientific).

Gene expression

The total RNA was extracted from cells, induced to osteogenic differentiation for 3, 10 and 20 days, using RNeasy Mini Kit (Qiagen) with a residual genomic DNA Eraser following the protocol. Then the RNA was subjected to reverse transcription using a SuperScript® III (Invitrogen, Life Technologies) following the manufacture's instructions. The resulting complementary DNA (cDNA) yield was then subjected to real-time polymerase chain reaction (RT-PCR) using an ABI PRISM 7000 Sequence Detention System (Applied Biosystems). The results were analyzed with Sequence Detector software (Applied Biosystems). Reaction solutions included SYBR Green Mastermix, 1 μM forward and reverse predesigned primers (Table S1, Supplementary information), and 10 μL cDNA template in a 30 μL volume. The cDNA samples were analyzed for expression of runt related transcription factor 2 (Runx-2), SP7 transcription factor, also known as osterix (Sp7/Osterix), alkaline phosphatase (Alp), and osteocalcin as bone gamma-carboxyglutamate protein (Bglap), relative to the β-actin (ACTB) as an internal standard for sample normalization.

Statistics

Statistical analysis was performed using Student's *t*-test and one-way analysis of variance with Dunnett's post-hoc testing, and significance was considered at a probability of $p<0.05$.

Results and Discussion

Characterization of NRL nanoparticles

At pH 7.4, the average particle size of NRL is around 300 nm with polydispersity index (*PDI*) of 0.25 at concentration of 10^{-4} wt% as revealed by DLS study (Fig. 1). The DLS data also shows that the distribution is clearly asymmetric. With increasing concentration up to 1.0 wt%, the clustered nanoparticle with a size of ~1300–5000 nm with *PDI* of ~0.5 was observed, indicating the nanoparticles are not stabilized electrostatically due to the weak ionic characteristics showing at pH 7.4.

Figure 2 shows the morphological feature of NRL nanoparticle at concentration of 10^{-4} wt% as revealed by FE-SEM image. The discrete particle exhibits very smooth surface having a size of ~300 nm (marked with the arrow in Fig. 2(a)). The aggregate formation consisting of many discrete particles during the removal of the water is also observed in which the particle size increases up to ~3 μm (Fig. 2(b)). The top surface is covered with molecules of protein thin layer that has both positively and negatively charged species like amino acid molecules. The NRL

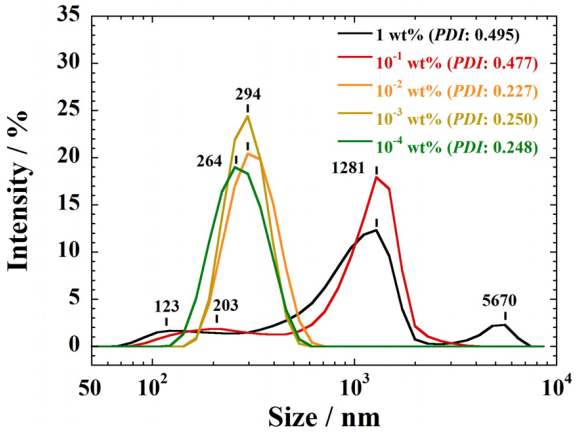

Figure 1. Particle size distribution with *PDI* of NRL in water at different concentrations ranged from 10^{-4}–1 wt% at pH 7.4.

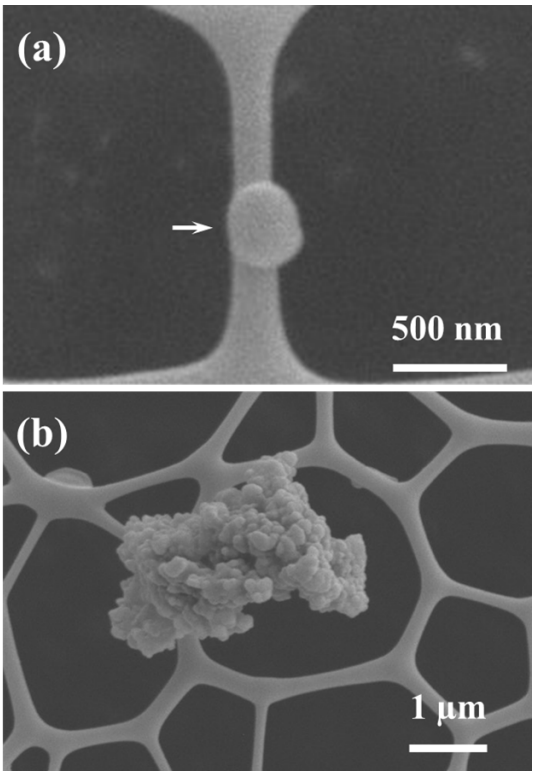

Figure 2. FE-SEM images showing NRL nanoparticles at concentration of 10^{-4} wt%: (a) discrete particle and (b) aggregate formation during the water removal.

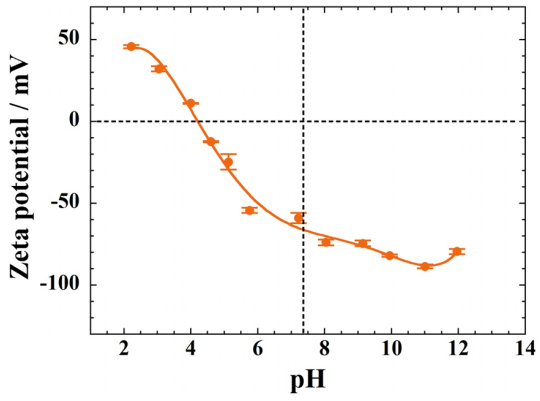

Figure 3. Zeta potential versus pH of NRL nanoparticles in water (0.01 wt%). Results are expressed as mean±S.D. (Standard deviation) (n=5).

nanoparticles have a variable of pH-dependent surface charge, because the amino acid residues can either acquire or lose protons depending on the pH of the ambient solution. For this reason, the total negative charge is provided∼−70 mV at pH 7.4 (indicated with the broken line). The point of zero charge is (pH) 4.1 (Fig. 3).

The cytotoxicity depends on the charge on the surface of the particles. Negatively charged particles at pH 7.40 show

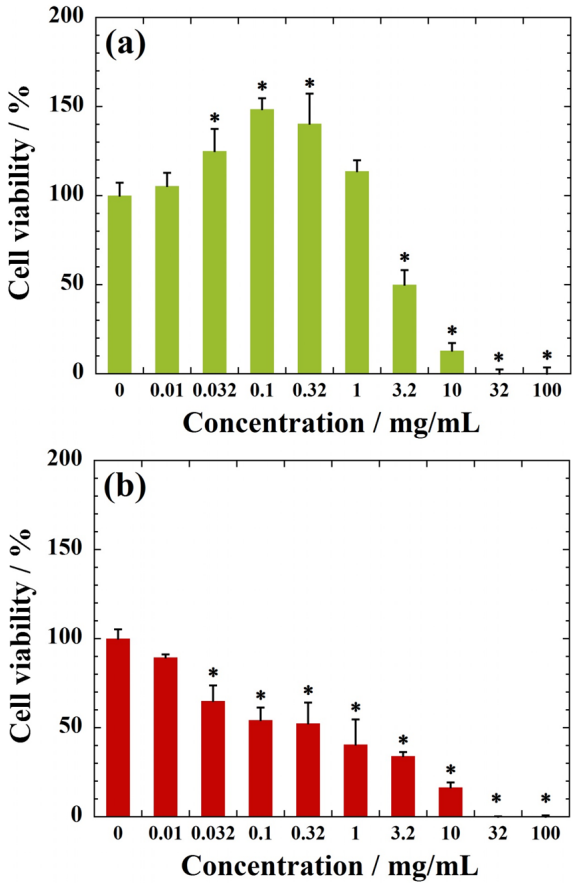

Figure 4. Cell viability as measured by WST-8 assay using (a) MC3T3-E1 and (b) A549 cells after 24 h of incubation with NRL nanoparticles of different concentrations.
Data were expressed as mean±S.D. (n=5). Note: * indicates p<0.05 compared with control.

lower unfavorable effect on the cells viability because of the negatively charged cell membrane (∼−20 mV), which plays an important role to separate the cytoplasm from the outside environment and modulate the movement of the particles in and out of the cell[11, 12].

Cytotoxicity of NRL nanoparticles

MC3T3-E1 cells are very sensitive to the NRL concentration, accompanied with high metabolic and dehydrogenase activity of the cells at concentration of less than 10.0 μg/mL. Beyond concentration of 10.0 μg/mL, NRL nanoparticles enhance MC3T3-E1 cell and viability in the range of 130–150% in comparison with the control (Fig. 4(a)). Experiments are underway to find out the actual reason behind this demonstration. This behavior will be deeply discussed further on the basis of the relation of endocytic process of the NRL nanoparticles into cells.

In contrast, the NRL nano particles are found to be toxic to the A549 cells (cell viabilities are below 60% at concen-

tration of 100 μg/mL) within 1 day (Fig. 4(b)). We need to consider the cell cycle regarding the suppression of proliferation (see Fig. 9(a)). The estimated IC_{50} values are 0.33 mg/mL for A549 cells and 3.99 mg/mL for MC3T3-E1 cells in the range of 10 μg/mL–10 mg/mL. The IC_{50} values for the ammonia are 1.19 mg/mL for MC3T3-E1 and 1.25 mg/mL for A549 cells, respectively (Fig. S1 and Table S2, Supplementary information), that is interpreted to mean that the ammonia does not exert an effect on cell viability in NRL suspensions for both cells. Our data show that the addition of even as much as 1.0 mg/mL of NRL nanoparticles in cell culture did not kill tested MC3T3-E1 cells. The NRL nanoparticles exposure to biological tissue is expected when one applies NRL as a carrier for anticancer drug delivery[13, 14].

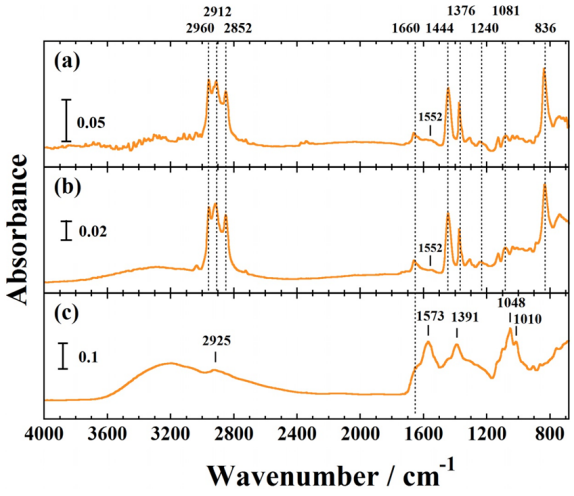

Figure 5. FTIR spectra of (a) NRL nanoparticles before fractionation, (b) fractionated NRL by ultra-centrifuge (rubber component), and (c) intermediate phase after fractionation in the region of 4000–680 cm^{-1}.

Fractionation of NRL nanoparticles and IC50

Figure 5(a) shows typical FTIR spectra of NRL nanoparticles before fractionation. The specific peaks of NRL are assigned. The sensitive bands at 2960 ($\nu_{as}(CH_3)$), 2912 (asymmetric stretching: $\nu_{as}(CH_2)$), 2852 (symmetric stretching: $\nu_s(CH_2)$), 1444, 1376 ($\delta(CH_3)$), 836 cm^{-1} (*cis*[>C=CH–]) are attributed to *cis*-1,4-polyisoprene. The sensitive bands at 1664 (amide: ν(C=O)), 1552 (amide: ν(C–N/N–H)), 1240 (asymmetric stretching: $\nu_{as}(PO_2^-)$), and 1081 cm^{-1} (symmetric stretching mode: $\nu_s(PO_2^-)$) are attributed to the molecules on the surface of NRL nanoparticles. A band located at 3300 cm^{-1} was assigned to the structural OH stretching mode (ν(OH)).

The fractionated NRL have previously been characterized the substances in latex in the largest amounts of proteins, lipids and inorganic salts[15]. The fractionated NRL by ultra-centrifuge in this study is composed of three constituents as aforementioned. The rubber component, content of approximately 94 wt%, shows both $\nu_{as}(PO_2^-)$ and $\nu_s(PO_2^-)$ bands assigned to lipids, and ν(C=O) is seen clearly due to the undissolved substance in water (Fig. 5(b)). The intermediate phase (5.8 wt%) corresponding to dissolved components in water, exhibits adsorbed proteins together with adsorbed phospholipids on the NRL surfaces (Fig. 5(c)). The remainder as a sediment (0.2 wt%) is non-rubber constituents such as inorganic ions and sterol glycosides[15].

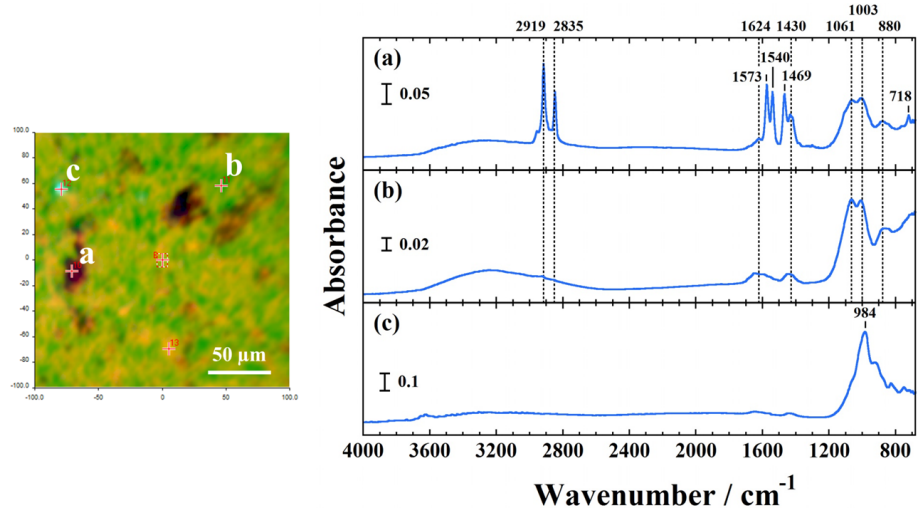

Figure 6. FTIR image of the ultra-centrifuged sediment obtained from the selected 200×200 μm^2 area (left panel). FTIR spectra of corresponding three constituents (a)–(c) by plotting PCA (right panel) in the region of 4000–680 cm^{-1}.

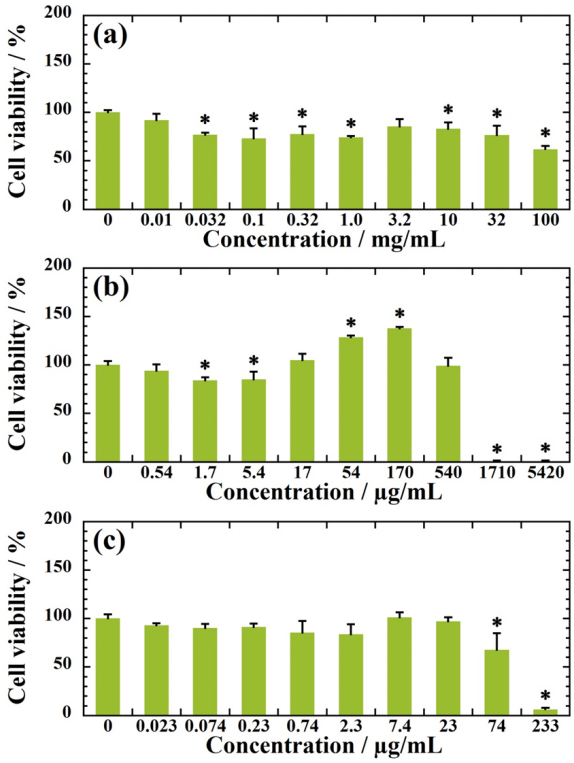

Figure 7. Cell viability as measured by WST-8 assay using MC3T3-E1 cell after 24 h of incubation with (a) rubber component, (b) intermediate phase, and (c) sediment of different concentrations after ultra-centrifuge. Data were expressed as mean±S.D. (n=5). Note: * indicates p<0.05 compared with control.

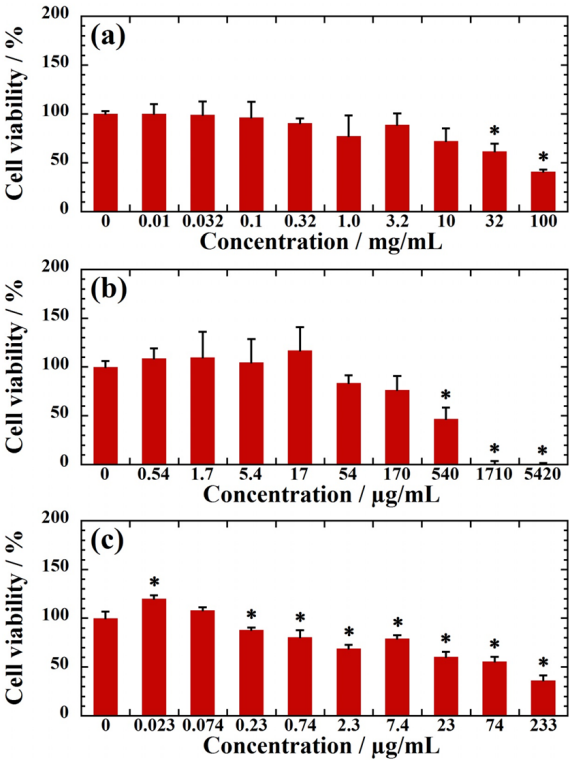

Figure 8. Cell viability as measured by WST-8 assay using A549 cell after 24 h of incubation with (a) rubber component, (b) intermediate phase, and (c) sediment of different concentrations after ultra-centrifuge. Data were expressed as mean±S.D. (n=5). Note: * indicates p<0.05 compared with control.

Table 1. EDX analysis of the ultracentrifuged sediment.

Elements	Fraction / wt%
Mg	4.6
P	4.31
S	0.25
K	0.25
Ca	0.16
Rb	0.007
Organic compounds	90.42

FTIR image is generated by plotting the principal components analysis (PCA) to illustrate the relative distribution of the components, as shown in Fig. 6 (left panel). The ultra-centrifuged sediment is divided into three different kinds of constituents as revealed by PCA (right panel in Fig. 6). Through EDS analysis for the sediment, the organic compounds corresponded to 90.42 wt%. The high contents of Mg and P, which were attributed to $MgNH_4PO_3$ $6(H_2O)$ were presented (Table 1). We calculated an Mg/P ratio of 1.36 within the range expected for struvite. The sensitive bands at 1061 cm^{-1} ($\nu_3(PO_4^{3-})$) and 1003 cm^{-1} ($\nu_3(PO_4^{3-})$) is attributed to the struvite, which is often found in lattices of low stability[16]. The peak occurs at 1573 cm^{-1} and the band at 1540 cm^{-1} corresponds to N–H in plane bending δ(N–H). The bands at 2919 cm^{-1} and 2835 cm^{-1} might be attributed to organic compounds (sterol glycoside-like hydrocarbons). Some potassium, calcium, rubidium, copper and zinc are associated with the rubber phase (Fig. S2, Supplementary information)[17, 18].

Although the information on them should be considered in more detail, the constituents of the sediment are unknown at present. However, the cytocompatibility analysis of the sediment has not been reported yet. Therefore the fractionated components on the cytotoxicity were measured against normal and cancer cells.

For MC3T3-E1cells incubation with rubber component (Fig. 7(a)), their viability is maintained at >60% for concentration up to 100 mg/mL, implying high biocompatibility of rubber component as compared with that of NRL nanoparticles. The IC_{50} value for MC3T3-E1 cells is more than 100 mg/mL. The intermediate phase induces the enhancement of MC3T3-E1 cellular proliferation and viability in the range of 110–140% (Fig. 7(b)), which is a similar characteristic with NRL nanoparticles as seen in Fig. 4(a).

Table 2. IC_{50} values of NRL and three components after ultra-centrifuge for MC3T3-E1 and A549 cells at 24 h.

Samples	MC3T3-E1 IC_{50}/mg/mL	A549 IC_{50}/mg/mL
NRL	3.99	0.33
Rubber component	N.D.[a]	82.6
Intermediate phase	1.07	0.41
Sediment	0.19	0.07

[a] The values are not detected.

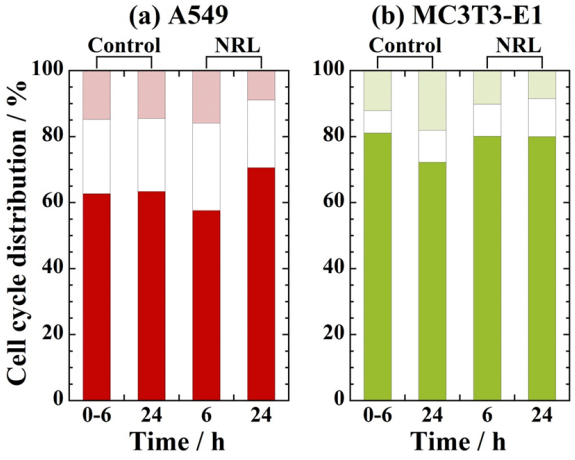

Figure 9. Cell cycle distribution of (a) A549 and (b) MC3T3-E1 cells after treated with NRL nanoparticles with concentration of 330 μg/mL (IC_{50} for A549) in G_0/G_1 (dark colors), S (white), and G_2/M (light colors) for 0–24 h. (n=3).

The incubation with sediment leads to a significant vitality reduction (7%) beyond concentration of 230 μg/mL for MC3T3-E1 cells (Fig. 7(c)).

For A549 cells incubation, the characteristics in cell viability show the same characteristics as compared with that cultured in presence of NRL nanoparticles (Fig. 8). With increasing each concentration for WST-8 test, a significant vitality reduction is observed in each constituent. The estimated IC_{50} values at 24 h for both cells are summarized in Table 2. The presence of the non-rubber constituents contributes to significant point of the cytotoxicity. An interesting point is the comparison of IC_{50} values for sediment in both cells. Almost three-fold higher in toxicity given on A549 cells is found after 24 h of incubation with non-rubber constituents (intermediate phase and sediment) when we compared to that of MC3T3-E1 cells. For NRL nanoparticles, the IC_{50} value for MC3T3-E1 cells is one order of magnitude higher in toxicity as compared to that of A549 cells (3.99 mg/mL for MC3T3-E1 and 0.33 mg/mL for A549 cells). The NRL nanoparticles exposure to biological bone tissue is expected when one applies nanoparticles for bone regeneration[13].

Cell cycle distribution

To understand the proliferation state the cell cycle distribution is shown in Fig. 9. PI discriminates cells at different stages of the cell cycle, based on different DNA content in the presence of RNAse to increase the specificity of DNA staining[19]. The cell proliferation is controlled by different phases such as the G_0/G_1 (containing two copies of each chromosome), S (synthesis of chromosomal DNA), G_2/M (doubled chromosomal DNA) phases. The A549 cells exhibits cell cycle arrest clearly at G_0/G_1 phase with incubation time from 6 to 24 h due to the cells exposed to IC_{50} value (0.33 mg/mL), as compared to that of control, where shows no observed notable difference in distribution up to 24 h (Fig. 9(a)). On the other hand, for MC3T3-E1 cells incubated with NRL nanoparticles (330 μg/mL<IC_{50}), the cell cycle remains almost constant in the G_0/G_1 phase for 24 h incubation, although the increment of the fraction of cells without NRL (control) is found in the G_2/M phase (Fig. 9(b)). It is clear from these cell cycle distributions that the effect of suppression on the proliferation for A549 cells seems to be different due to the significant difference in cytotoxicity of NRL nanoparticles in the medium.

The prolonged G_0/G_1 event occurs at incubation with NRL, which indicates the presence of apoptotic cells. The level of cell apoptosis was examined by caspases 3/7 staining. Caspases (cysteinyl-directed aspartate-specific proteases) are cysteine proteases that play a central role in propagating the process of programmed cell death (apoptosis) in response to proapoptotic signals. Thus, activation of caspase-3/7 is a hallmark of an early event during apoptotic process.

After 24 h of incubation with NRL (0.33 mg/mL=IC_{50}), intermediate (0.14 mg/mL=IC_{50}), and/or sediment (0.07 mg/mL=IC_{50}), A549 cells show an increase on the percentage of apoptotic cells (ca. 5%) in comparison with control (Fig. S3, Supplementary information). This indicates the rather strong apoptosis induce effect on A549 cells. At the same time, late apoptosis or necrosis is rather prominent in the cells incubated with NRL (ca. 3% of the total cells). The A549 cells treated with intermediate and/or sediment show no significant increase on the percentage of apoptotic cells.

Gene expression and matrix mineralization of MC3T3-E1 cells

The gene expression of Runx-2, Sp7/Osterix, alkaline phosphatase (Alp), and osteocalcin (Bglap) relative to houkeeping gene (ACTB) were determined by RT-PCR at day 3, day 10 and day 20. The NRL nanoparticles show relatively stable expression of Runx-2 from 3 days to 20 days

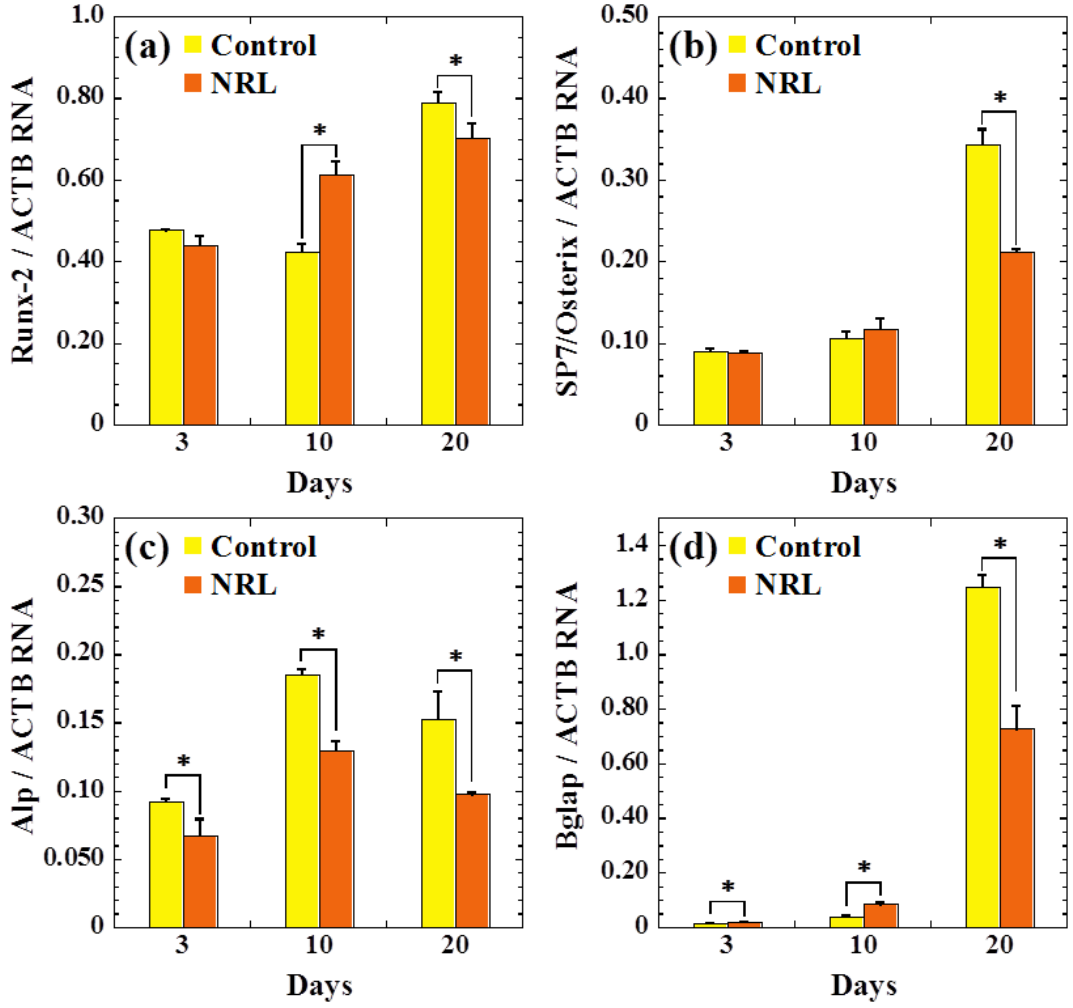

Figure 10. RT-PCR analysis of the osteogenic gene expression of (a) Runx-2, (b) Sp7/Osterix, (c) Alp, and (d) Bglap for MC3T3-E1 cells cultured with NRL nanoparticles of 1.0 mg/mL at day 3, day 10 and day 20.
Data were expressed as mean±S.D. (n=3). Note: * indicates p<0.05 compared with control (Student's t-test).

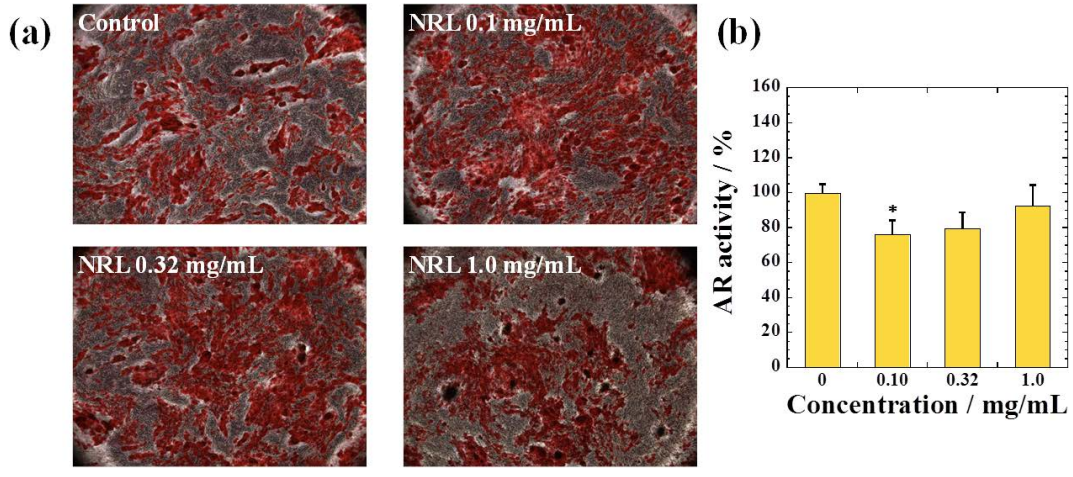

Figure 11. (a) Alizarin Red staining and (b) semi-quantitative evaluation of calcium deposition by MC3T3-E1 cells cultured with different NRL nanoparticle concentration after 20 days.
Data were expressed as mean±S.D. (n=4). Note: * indicates p<0.05 compared with control.

(Fig. 10(a)). The MC3T3-E1cells on mineralized matrices exhibits higher expression of Runx-2 for the late stage of osteogenic differentiation (at day 20). But there are significant differences between NRL-loaded sample (1.0 mg/mL) and control throughout 20 days of culture. The Sp7/Osterix is also considered as a marker for the early stage osteogenic differentiation[20]. The expression of Sp7/Osterix is lower in the NRL-loaded sample at day 20 (Fig. 10(b)). This shows the same trend with Runx-2. This effect is further confirmed by the expression of the Alp gene, which is a marker ranged from the early to intermediate stages in osteogenic differentiation of MC3T3-E1 cells (Fig. 10(c)). The expression of Alp gene is elevated up to day 10 and has a decreasing trend from 10 days to 20 days. The Bglap gene is a typical marker for the late stage of osteogenic differentiation. The NRL nanoparticles promote the osteogenic differentiation earlier than control at day 10 and have decreasing trend at day 20 (Fig. 10(d)).

To examine matrix mineralization, 20 days cultures were fixed and stain by Alizarin Red solution (Fig. 11(a)), which stains calcium deposits as another marker of osteogenic differentiation. Interestingly, for osteogenic differentiation of MC3T3-E1 cells, there are no statistical differences in absorbance between any of samples except for NRL nanoparticles with loading of 0.1 mg/mL, on which a slightly lower than the control, as shown in Fig. 11(b).

The MC3T3-E1 cells cultured with lower NRL concentration (0.1 mg/mL and 0.32 mg/mL) showed more stable gene expression compared with that of high loaded sample (Fig. S4, Supplementary information). These results indicate that the NRL nanoparticles did not cause so significant changes in osteogenic differentiation on the different concentration of the nanoparticles in the range of <0.32 mg/mL.

In addition, we have successfully prepared the biocomposites composed of NRL and bone tissue. Taking together the calcium deposition and gene expression, the results show promise of the NRL nanoparticle for application in bone engineering.

Conclusions

The present study has examined the cytotoxicity of NRL nanoparticles for cultured mouse calvaria preosteoblastic cells (MC3T3-E1) and human alveolar basal epithelial (A549) cells. For MC3T3-E1 cells, we found that the higher cytocompatibility of NRL nanoparticles without a significant vitality reduction for concentration up to 1000 μg/mL. The estimated IC_{50} value was an order of magnitude higher as compared to that of A549 cells. We have successfully fractionated NRL nanoparticles by ultra-centrifuge and obtained three constituents, i.e., rubber component, intermediate phase and sediment. The presence of the non-rubber constituents dominantly affected the cytotoxicity. The effect of suppression on the proliferation for A549 cells seemed to be different due to the significant difference in cytotoxicity of NRL nanoparticles in the medium as revealed by cell cycle distributions. After 20 days of cultured with osteogenic supplement, both rather stable gene expression and calcium deposition were observed from MC3T3-E1 cells cultured with NRL nanoparticles. We have successfully prepared the biocomposites composed of NRL and bone tissue.

Author Contributions

The manuscript was written through contributions of all authors. All authors have given approval to the final version of the manuscripts.

Notes

The authors declare no competing financial interest.

Acknowledgments

This work was supported by the Grant in TTI as a Special Research Project (2014).

References

1) Ereno C., Catanzaro Guimaraes S. A., Pasetto S., Herculano R. D., Silva C. P., Graeff C. F. O., Tavano O., Baffa O., Kinoshita A.: *J. Biomed. Mater. Res. A.*, **95A**, 932–939 (2010).
2) Herculano R. D., Silva C. P., Ereno C., Catanzaro Guimaraes S. A., Kinoshita A. de Oliveira Graeff C. F.: *Mater. Res.*, **12**, 253–256 (2009).
3) Sampaio R. B., Mendonca R. J., Simioni A. R., Costa R. A., Siqueira R. C., Correa V. M., Tedesco A. C., Haddad A., Coutinho Netto J., Jorge R.: *Current Eye Research.*, **35**, 56–62 (2010).
4) Ferreira M., Mendonç R. J., Coutinho-Netto J., Mulato M.: *Braz. J. Phy.*, **39**, 564–569 (2009).
5) Balabanian C. A., Coutinho-Netto J., Lamano-Carvalho T. L., Lacerda S. A., Brentegani L. G.: *J. Oral Sci*., **48**, 201–205 (2006).
6) Anancharungsuk W., Polpanich D., Jangpatarapongsa K., Tangboriboonrat P.: *Colloid Surf. B*., **78**, 328–333 (2010).
7) Valodkar M., Jadeja R. N., Thounaojam M. C., Devkar R. V., Thakore S.: *Mater. Sci. Eng. C*., **31**, 1723–1728 (2011).
8) Baek H. S., Yoo J. Y., Rah D. K., Han D. W., Lee D. H., Kwon O. H., Park J. C.: *Yonsei Med. J.*, **46**, 579–583 (2005).
9) Stephansson S. N., Byers B. A., García A. J.: *Biomaterials*, **23**, 2527–2534 (2002).

10) Nishida Y., Domura R., Sakai R., Okamoto M., Arakawa S., Ishiki R., Salick M. R., Turng L.: *Polymer*, **56**, 73–81 (2015).
11) Bondar O. V., Saifullina D. V., Shakhmaeva I. I., Mavlyutova I. I., Abdullin T. I.: *Acta Naturae*, **4**(1(12)), 78–81 (2012).
12) Xiao K., Li Y., Luo J., Lee J. S., Xiao W., Gonik A. M, Agarwal R. G., Lam K. S.: *Biomaterials*, **32**, 3435–3446 (2011).
13) Borges F. A., de Almeida Filho E., Miranda M. C., dos Santos M. L., Herculano R. D., Guastaldi A. C.: *J. Biomater. Sci. Polym. Ed*., **26**, 1256–1268 (2015).
14) Furuya M., Shimono N., Yamazaki K., Domura R., Okamoto M.: *Mater. Today Chem*., **5**, 63–71 (2017).
15) Archer B. L., Barnard D., Cockbain E. G., Dickenson P. B., McMullen A. I.: "The Chemistry and Physics of Rubberlike Sbubstances", Eds. Bateman L., Maclaren S., London, Wiley, New York (1963), Chapter 3.
16) Beaufils E. R.: *Proc. 3rd Rubb. Tech. Conf.*, London, 87 (1954).
17) Belmas R.: *Rubber Chem. Technol.*, **25**, 124–132 (1952).
18) Flint C. F., Ramage H.: *Chem. Ind.*, **54**, 337 (1935).
19) Darzynkiewicz Z., Gloria J. G., Bedner E.: *Curr. Protoc. Cell Biol*., 8.4.1–8.4.18 (2001).
20) Choi J. Y., Lee B. H., Song K. B., Park R. W., Kim I. S., Sohn K. Y., Jo J. S., Ryoo H. M.: *J. Cell Biochem.*, **61**, 609–618 (1996).